Improved Full-Vectorial Finite-Difference Mode Solver for Optical Waveguides With Step-Index Profiles

Yen-Chung Chiang, Yih-Peng Chiou, and Hung-Chun Chang, *Senior Member, IEEE*

***Abstract*—A general relation considering an interface condition between a sampled point and its nearby points in the finite-difference analysis of optical waveguides is derived. Our formulation is a full-vectorial one, and the interface can be oblique to the global coordinate axes or even can be with curvature. Using the derived formulation, optical waveguide structures with arbitrary step-index profiles can be dealt with. The validity of the proposed method is examined by comparing the numerical calculation with the analytical solution of a step-index optical fiber. The method is also applied to the analysis of fused fiber-optic couplers and compared with prior analysis using the surface integral equation method.**

***Index Terms*—Finite-difference method, full vectorial mode solver, fused fiber couplers, step-index optical waveguides.**

I. Introduction

DIELECTIC optical waveguides such as fiber waveguides, buried rectangular waveguides, and rib waveguides have played an important role in the design of optical devices and systems. With the rapid progress of computers, in both software and hardware, a relatively low-cost and highly accurate method to design or predict the performance of an optoelectronic device is to make use of the simulation programs or computer-aided design (CAD) tools. Among these CAD tools, the finite-difference method (FDM) has become an attractive numerical method for analyzing optical waveguides because of the simplicity of its implementation and the sparsity of its resultant matrix.

For the dielectric waveguides mentioned above, it is quite usual that the structure is piecewise homogeneous and thus contains a step refractive index profile. A general cross-sectional view of the structure is shown in Fig. 1(a). The complete solution of the electromagnetic fields for such a problem is generally vectorial rather than scalar or semivectorial. Since the differential equations are approximated with their corresponding finite-difference equations in the FDM, the efficiency and accuracy of the FDM are greatly affected by its finite-difference (FD) formulas. The simplest FD formula is based on the scalar approximation and it may not be sufficiently accurate when the polarization-dependent characteristics of the structure need to be taken into account. Over the years, many approaches have been proposed to improve the efficiency and accuracy of the FDM, including semivectorial [1]–[3] and full-vectorial [4]–[8] formulations. In those formulations, the vectorial analysis usually starts from the following equation derived from Maxwell's equations:

$$\begin{bmatrix} P_{xx} & P_{xy} \\ P_{yx} & P_{yy} \end{bmatrix} \begin{bmatrix} E_x \\ E_y \end{bmatrix} = \beta^2 \begin{bmatrix} E_x \\ E_y \end{bmatrix} \tag{1}$$

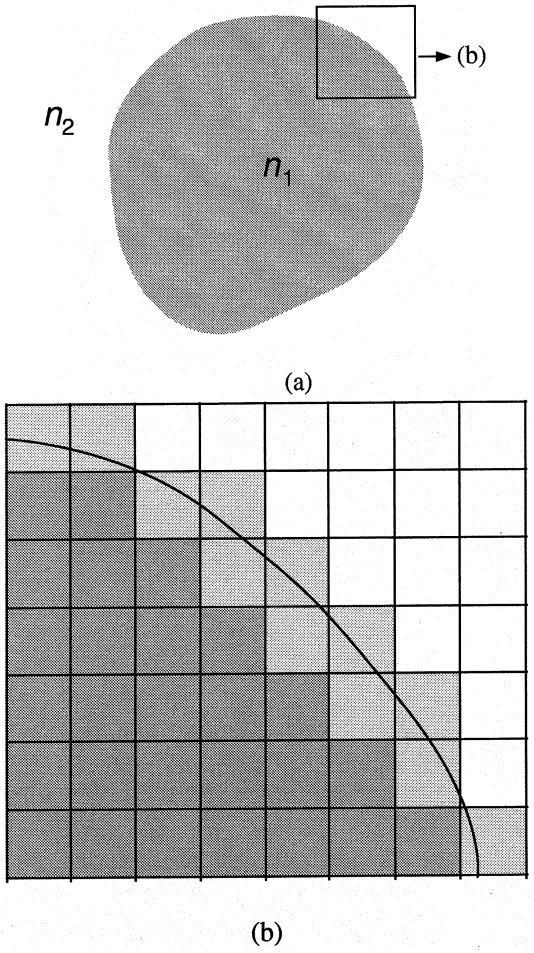

Fig. 1. (a) Cross section of the problem under consideration. (b) Stair-case approximation for the oblique interface.

Manuscript received August 29, 2001; revised February 11, 2002. This work was supported by the National Science Council of the Republic of China under Grant NSC89-2218-E-002-093 and Grant NSC90-2215-E-002-040.

Y.-C. Chiang is with the Department of Electrical Engineering, National Taiwan University, Taipei 106-17, Taiwan, R.O.C.

Y.-P. Chiou was with the Department of Electrical Engineering, National Taiwan University. He is now with Rsoft Inc., Ossining, NY 10562 USA.

H.-C. Chang is with the Department of Electrical Engineering, the Graduate Institute of Electro-Optical Engineering, and the Graduate Institute of Communication Engineering, National Taiwan University, Taipei 106-17, Taiwan, R.O.C.

Digital Object Identifier 10.1109/JLT.2002.800292

where the differential operators are defined as

$$P_{xx}E_x = \frac{\partial}{\partial x}\left(\frac{1}{n^2}\frac{\partial(n^2E_x)}{\partial x}\right) + \frac{\partial^2 E_x}{\partial y^2} + n^2k_0^2E_x \quad (2)$$

$$P_{yy}E_y = \frac{\partial^2 E_y}{\partial x^2} + \frac{\partial}{\partial y}\left(\frac{1}{n^2}\frac{\partial(n^2E_y)}{\partial y}\right) + n^2k_0^2E_y \quad (3)$$

$$P_{xy}E_y = \frac{\partial}{\partial x}\left(\frac{1}{n^2}\frac{\partial(n^2E_y)}{\partial y}\right) - \frac{\partial^2 E_y}{\partial x \partial y} \quad (4)$$

$$P_{yx}E_x = \frac{\partial}{\partial y}\left(\frac{1}{n^2}\frac{\partial(n^2E_x)}{\partial x}\right) - \frac{\partial^2 E_x}{\partial y \partial x} \quad (5)$$

where β is the modal propagation constant, n is the transverse refractive-index function, and k_0 is the free-space wavenumber. Note that $P_{xx} \neq P_{yy}$ causes the polarization dependence, whereas $P_{xy} \neq 0$ or $P_{yx} \neq 0$ induce polarization coupling between E_x and E_y. Conventional FD schemes are obtained by directly discretizing (1)–(5) with the graded-index approximation at the interface. The graded-index approximation assumes that the transverse refractive-index function n is graded varying and continuous across the interface. The conventional FDMs are generally arranged in such a way that the fields are continuous in the first partial differential operation in order to avoid the discontinuity problem at the interface. However, the second-order partial differential operation still can only be approximated by the graded-index assumption. Recently, some modified treatments have been presented to deal with optical waveguides with step-index profiles [2], [3], [8], [9], including our former work dealing with the planar waveguide case [9]. Most of the improved formulas have been constrained to semivectorial cases. Although some of them are full-vectorial in nature, in those formulations the improved FD formulas were still substituted back into the above equations based on the graded-index approximation in order to evaluate the coupling term between the two polarization components of the field [8].

Besides the step-index interface problem, the rectangular meshes usually used in the FDM cause another problem in the FDM when the structure contains oblique or curved interfaces, as shown in Fig. 1(b). The conventional treatment is to use either the graded-index approximation or the stair-case index approximation. Vassallo [2] derived an improved FD formulation considering an oblique interface, but the formulation is only suitable for the scalar case and the truncation error is of the first order at best. In his treatment of the semivectorial case, the structures were only allowed to have discontinuities directed along either the x or y axes, just like other semivectorial formulations.

In this paper, we will derive improved FD formulations which can treat optical waveguides with step-index profiles. The formulations are full-vectorial ones and the interface can be oblique to the x and y axes or can even be curved. Our process of derivation is similar to Vassallo's [2] in that we employ the Taylor series expansion and match the interface conditions. To obtain a full-vectorial formulation that can treat the oblique interface, we further introduce the local coordinate transformation and derive rigorous expressions for the interface conditions in the locally transformed coodinate. We also find that, through matching interface conditions, the coupling between the two transverse polarization components of the field will be automatically included in the resultant FD formulas.

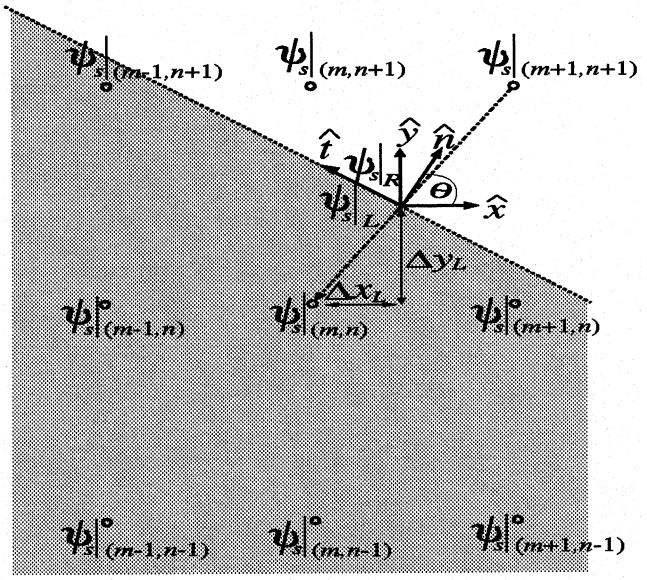

Fig. 2. Cross section of the problem under consideration for a linear oblique interface.

The derivations of our formulations are given in Section II, followed by a description of numerical implementation in Section III. Some numerical results are presented in Section IV for verifying the validity of our formulations. We apply our improved formulation into the multimode optical fiber, and the results show that our formulation converges to the exact analytical solution very well in both the weakly and strongly guiding cases. We also apply our new formulations into the fused optical fiber coupler; in this case, we compare the results with those computed using the surface integral equation method (SIEM) and find good agreement between the two kinds of methods. The conclusion is drawn in Section V.

II. Formulation

A general relation between the field $\psi_s|_{(m,n)}$, $s = x$ or y, at the sampled point (m,n) and the fields nearby, as shown in Fig. 2 for a linear oblique interface or as shown in Fig. 3 for a curved interface, is derived in this section. The quantities $\psi_x|_{(m,n)}$ and $\psi_y|_{(m,n)}$, respectively, denote the transverse magnetic fields H_x and H_y or the transverse electric fields E_x and E_y at the sampled point (m,n).

A. Linear Oblique Interface Case

Consider a linear oblique interface between two dielectric regions with different refractive indexes, as shown in Fig. 2, with the normal and tangential unit vectors, denoted as $\hat{n}$ and $\hat{t}$, respectively. $\psi_s|_L$ and $\psi_s|_R$ shown in Fig. 2 represent the fields at just to the left and right sides of the interface, respectively, between the two sampled points (m,n) and $(m+1,n+1)$. We will derive the relationship between the fields $\psi_s|_{(m,n)}$ and $\psi_s|_{(m+1,n+1)}$. The problem under consideration is piecewise homogeneous, and we can employ the two-dimensional (2-D)

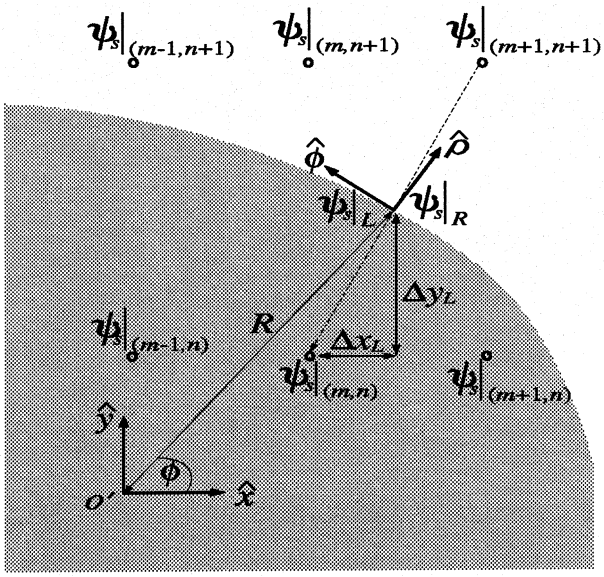

Fig. 3. Cross section of the problem under consideration for a curved interface.

Taylor series expansion within the homogeneous region and express $\psi_s|_L$ in terms of $\psi_s|_{(m,n)}$ and its derivatives as

$$\psi_s|_L = \psi_s|_{(m,n)} + \Delta x_L \left.\frac{\partial \psi_s}{\partial x}\right|_{(m,n)} + \Delta y_L \left.\frac{\partial \psi_s}{\partial y}\right|_{(m,n)} + \frac{\Delta x_L^2}{2!} \left.\frac{\partial^2 \psi_s}{\partial x^2}\right|_{(m,n)} + \frac{2\Delta x_L \Delta y_L}{2!} \left.\frac{\partial^2 \psi_s}{\partial x \partial y}\right|_{(m,n)} + \frac{\Delta y_L^2}{2!} \left.\frac{\partial^2 \psi_s}{\partial y^2}\right|_{(m,n)} + \frac{\Delta x_L^3}{3!} \left.\frac{\partial^3 \psi_s}{\partial x^3}\right|_{(m,n)} + \cdots \quad (6)$$

where Δx_L and Δy_L are as shown in Fig. 2. By differentiating (6) with respect to x or y, we have

$$\left.\frac{\partial \psi_s}{\partial x}\right|_L = \left.\frac{\partial \psi_s}{\partial x}\right|_{(m,n)} + \Delta x_L \left.\frac{\partial^2 \psi_s}{\partial x^2}\right|_{(m,n)} + \Delta y_L \left.\frac{\partial^2 \psi_s}{\partial x \partial y}\right|_{(m,n)} + \frac{\Delta x_L^2}{2!} \left.\frac{\partial^3 \psi_s}{\partial x^3}\right|_{(m,n)} + \cdots \quad (7)$$

$$\left.\frac{\partial \psi_s}{\partial y}\right|_L = \left.\frac{\partial \psi_s}{\partial y}\right|_{(m,n)} + \Delta x_L \left.\frac{\partial^2 \psi_s}{\partial x \partial y}\right|_{(m,n)} + \Delta y_L \left.\frac{\partial^2 \psi_s}{\partial y^2}\right|_{(m,n)} + \frac{\Delta x_L^2}{2!} \left.\frac{\partial^3 \psi_s}{\partial x^2 \partial y}\right|_{(m,n)} + \cdots \quad (8)$$

The higher order derivatives of $\psi_s|_L$ can thus be obtained in terms of the derivatives of $\psi_s|_{(m,n)}$ by successively differentiating (7) and (8) with respect to x or y and written in a matrix form as

$$\begin{bmatrix} \psi_s|_L \\ \left.\frac{\partial \psi_s}{\partial x}\right|_L \\ \left.\frac{\partial \psi_s}{\partial y}\right|_L \\ \left.\frac{\partial^2 \psi_s}{\partial x^2}\right|_L \\ \left.\frac{\partial^2 \psi_s}{\partial x \partial y}\right|_L \\ \vdots \end{bmatrix} = \begin{bmatrix} 1 & \Delta x_L & \Delta y_L & \frac{\Delta x_L^2}{2!} & \Delta x_L \Delta y_L & \cdots \\ 0 & 1 & 0 & \Delta x_L & \Delta y_L & \cdots \\ 0 & 0 & 1 & 0 & \Delta x_L & \cdots \\ 0 & 0 & 0 & 1 & 0 & \cdots \\ 0 & 0 & 0 & 0 & 1 & \cdots \\ \vdots & \vdots & \vdots & \vdots & \ddots & \vdots \\ 0 & 0 & 0 & 0 & 0 & 1 \end{bmatrix} \cdot \begin{bmatrix} \psi_s|_{(m,n)} \\ \left.\frac{\partial \psi_s}{\partial x}\right|_{(m,n)} \\ \left.\frac{\partial \psi_s}{\partial y}\right|_{(m,n)} \\ \left.\frac{\partial^2 \psi_s}{\partial x^2}\right|_{(m,n)} \\ \left.\frac{\partial^2 \psi_s}{\partial x \partial y}\right|_{(m,n)} \\ \vdots \end{bmatrix} + \text{H.O.T.} \quad (9)$$

where H.O.T. denotes "higher order terms." By assembling $\psi_x|_L$ and $\psi_y|_L$ and their derivatives into a vector, $\overline{\Psi}_L = [\psi_x|_L, \partial\psi_x/\partial x|_L, \partial\psi_x/\partial y|_L, \partial^2\psi_x/\partial x^2|_L, \ldots, \psi_y|_L, \partial\psi_y/\partial x|_L, \partial\psi_y/\partial y|_L, \partial^2\psi_y/\partial x^2|_L, \ldots]^t$, where the superscript t denotes "transpose," (9) leads to

$$\overline{\Psi}_L = \overline{\overline{M}}_{L:(m,n)} \cdot \overline{\Psi}_{(m,n)} + \text{H.O.T.} \quad (10)$$

where the vector $\overline{\Psi}_{(m,n)}$ is composed of $\psi_x|_{(m,n)}$, $\psi_y|_{(m,n)}$, and their derivatives in the same manner as $\overline{\Psi}_L$. Similarly, by expressing $\psi_s|_{(m+1,n+1)}$ in terms of $\psi_s|_R$ and its derivatives, we have

$$\overline{\Psi}_{(m+1,n+1)} = \overline{\overline{M}}_{(m+1,n+1):R} \cdot \overline{\Psi}_R + \text{H.O.T.} \quad (11)$$

where $\overline{\Psi}_R$ is similarly defined as for $\overline{\Psi}_L$ and $\overline{\Psi}_{(m,n)}$, and

$$\overline{\Psi}_{(m+1,n+1)} = [\psi_x|_{(m+1,n+1)}, 0, 0, \ldots, \psi_y|_{(m+1,n+1)}, 0, 0, \ldots]^t.$$

The number of elements of the vector $\overline{\Psi}_{(\cdot)}$ is determined by the order of the truncation error we desire in the formulation. The choice of grid points used in our formulations decides which derivative terms should be included in the vector $\overline{\Psi}_{(m,n)}$. In this paper, the truncation error is of order two and we choose nine points as shown in Fig. 2, and thus the number of elements is 18. It is worth noticing that, under such a choice of mesh points, the elements of $\overline{\Psi}_{(m,n)}$ cannot contain derivative terms of the field which are higher than the third partial differentiation in the either x or y direction, since such terms will make the resultant matrix become singular.

We next make a coordinate transformation by rotating the x-y coordinate at the interface to the coordinate with the unit vectors $\hat{n}$ and $\hat{t}$, as shown in Fig. 2, as the bases. Using the relations

$$\begin{aligned} \hat{x} &= \cos\theta \cdot \hat{n} - \sin\theta \cdot \hat{t} \\ \hat{y} &= \sin\theta \cdot \hat{n} + \cos\theta \cdot \hat{t} \\ \frac{\partial}{\partial x} &= \cos\theta \cdot \frac{\partial}{\partial n} - \sin\theta \cdot \frac{\partial}{\partial t} \\ \frac{\partial}{\partial y} &= \sin\theta \cdot \frac{\partial}{\partial n} + \cos\theta \cdot \frac{\partial}{\partial t} \\ &\vdots \end{aligned}$$

$\overline{\Psi}_L$ is transformed into $\hat{\overline{\Psi}}_L$ through

$$\hat{\overline{\Psi}}_L = \overline{\overline{M}}_{CL} \cdot \overline{\Psi}_L \quad (12)$$

where $\hat{\overline{\Psi}}_L$ is a vector composed of $\psi_n|_L$, $\psi_t|_L$, and their n- and t-derivatives. Similarly, if we transform from the n-t coordinate back to the x-y coordinate system, it is expressed as

$$\overline{\Psi}_R = \overline{\overline{M}}_{RC} \cdot \hat{\overline{\Psi}}_R. \quad (13)$$

We need to link the vector $\widehat{\Psi}_L$ at one side of the interface with the vector $\widehat{\Psi}_R$ at the other side. The interface conditions require that

$$\begin{aligned}
H_n|_R &= H_n|_L \\
H_t|_R &= H_t|_L \\
\left.\frac{\partial H_n}{\partial n}\right|_R &= \left.\frac{\partial H_n}{\partial n}\right|_L \\
\left.\frac{\partial H_n}{\partial t}\right|_R &= \left.\frac{\partial H_n}{\partial t}\right|_L \\
\left.\frac{\partial H_t}{\partial n}\right|_R &= \frac{\epsilon_R}{\epsilon_L}\left.\frac{\partial H_t}{\partial n}\right|_L + \left(1-\frac{\epsilon_R}{\epsilon_L}\right)\left.\frac{\partial H_n}{\partial t}\right|_L \\
\left.\frac{\partial H_t}{\partial t}\right|_R &= \left.\frac{\partial H_t}{\partial t}\right|_L \\
\left.\frac{\partial^2 H_n}{\partial n^2}\right|_R &= \left.\frac{\partial^2 H_n}{\partial n^2}\right|_L + k_0^2(\epsilon_L-\epsilon_R)H_n|_L \\
\left.\frac{\partial^2 H_t}{\partial n^2}\right|_R &= \left.\frac{\partial^2 H_t}{\partial n^2}\right|_L + k_0^2(\epsilon_L-\epsilon_R)H_t|_L \\
&\vdots
\end{aligned}$$

for the magnetic fields and

$$\begin{aligned}
E_n|_R &= \frac{\epsilon_L}{\epsilon_R}E_n|_L \\
E_t|_R &= E_t|_L \\
\left.\frac{\partial E_n}{\partial n}\right|_R &= \left.\frac{\partial E_n}{\partial n}\right|_L \\
\left.\frac{\partial E_n}{\partial t}\right|_R &= \frac{\epsilon_L}{\epsilon_R}\left.\frac{\partial E_n}{\partial t}\right|_L \\
\left.\frac{\partial E_t}{\partial n}\right|_R &= \left.\frac{\partial E_t}{\partial n}\right|_L + \left(\frac{\epsilon_L}{\epsilon_R}-1\right)\left.\frac{\partial E_n}{\partial t}\right|_L \\
\left.\frac{\partial E_t}{\partial t}\right|_R &= \left.\frac{\partial E_t}{\partial t}\right|_L \\
\left.\frac{\partial^2 E_n}{\partial n^2}\right|_R &= \frac{\epsilon_L}{\epsilon_R}\left.\frac{\partial^2 E_n}{\partial n^2}\right|_L + \frac{k_0^2\epsilon_L(\epsilon_L-\epsilon_R)}{\epsilon_R}E_n|_L \\
\left.\frac{\partial^2 E_t}{\partial n^2}\right|_R &= \left.\frac{\partial^2 E_t}{\partial n^2}\right|_L + k_0^2(\epsilon_L-\epsilon_R)E_t|_L \\
&\vdots
\end{aligned}$$

for the electric fields, where ϵ_L and ϵ_R are the permittivities on the left-hand and right-hand sides of the interface, respectively. In either case, it is expressed as

$$\widehat{\Psi}_R = \overline{\overline{M}}_{RL}\cdot\widehat{\Psi}_L \tag{14}$$

with $\overline{\overline{M}}_{RL}$ corresponding to the above interface conditions of the magnetic field or the electric field. The above interface conditions are derived from boundary conditions for the fields, the divergence and curl Maxwell equations, and the Helmholtz equation. It is worth noticing that the x and y components of the fields at the interface are coupled to each other via the interface conditions.

Finally, by combining (10)–(14), we obtain

$$\overline{\Psi}_{(m+1,n+1)} = \overline{\overline{M}}_{(m+1,n+1)}\cdot\overline{\Psi}_{(m,n)} + \text{ H.O.T.} \tag{15}$$

where

$$\overline{\overline{M}}_{(m+1,n+1)} = \overline{\overline{M}}_{(m+1,n+1):R}\cdot\overline{\overline{M}}_{RC}\cdot\overline{\overline{M}}_{RL}\cdot\overline{\overline{M}}_{CL}\cdot\overline{\overline{M}}_{L:(m,n)}. \tag{16}$$

The relation between the above-mentioned fields and their derivatives can be illustrated as

$$\begin{aligned}
\psi|_{(m+1,n+1)} &\xleftarrow[\overline{\overline{M}}_{(m+1,n+1):R}]{\text{TSE}} \psi|_R \xleftarrow[\overline{\overline{M}}_{RC}]{\text{LCT}} \hat{\psi}\Big|_R \\
&\xleftarrow[\overline{\overline{M}}_{RL}]{\text{MBC}} \hat{\psi}\Big|_L \xleftarrow[\overline{\overline{M}}_{CL}]{\text{LCT}} \psi|_L \xleftarrow[\overline{\overline{M}}_{L:(m,n)}]{\text{TSE}} \psi|_{(m,n)}
\end{aligned}$$

where TSE denotes Taylor series expansion, LCT denotes local coordinate transformation, and MBC denotes matching the boundary conditions. Equation (16) connects the fields at the nearby point $(m+1,n+1)$ with the fields ψ_x and ψ_y and their derivatives at the sampled mesh point (m,n). Similarly, the fields at other nearby points $(m-1,n+1)$, $(m,n+1),\ldots$ can be expressed as the linear combanations of the fields and their derivatives at point (m,n). For our new FD formulation with $O(h^2)$ truncation error, we choose nine points in the formulation domain for derivation. By assembling the fields at the nine mesh points into a vector, $\widetilde{\Psi} = [\psi_x|_{(m-1,n+1)}, \psi_x|_{(m,n+1)}, \psi_x|_{(m+1,n+1)}, \cdots \psi_x|_{(m+1,n-1)}, \psi_y|_{(m-1,n+1)}, \cdots \psi_y|_{(m,n-1)}, \psi_y|_{(m+1,n-1)}]^t$, we can obtain the following equations from the relations similar to (16) connecting the fields and their derivatives at the sampled point (m,n) with the fields at the nearby eight points:

$$\widetilde{\Psi} = \widetilde{M}\cdot\overline{\Psi}_{(m,n)}. \tag{17}$$

Since the vector $\overline{\Psi}_{(m,n)}$ contains the quantities $\partial^2\psi_x/\partial x^2$, $\partial^2\psi_x/\partial y^2$, $\partial^2\psi_y/\partial x^2$, and $\partial^2\psi_y/\partial y^2$ at the sampled point (m,n), if we take the inverse operation of (17), a new set of FD formulas can be obtained as the linear conbinations of the fields at the nine mesh points. The coupling between the two polarizations of fields will be automatically included in these FD formulas if the interface exists, and we do not need to evaluate the coupling terms by the graded approximation formulation expressed in (4) and (5), as was done in [4], [7], and [8].

B. The Curved Interface Case

If the interface is curved with the normal and tangential unit vectors $\hat{\rho}$ and $\hat{\phi}$, respectively, as shown in Fig. 3, the formulations can be further modified. Let the curvature of the interface be κ or the effective radius be $R = 1/\kappa$. A similar process to what we did in the linear oblique interface case can be derived. The process of Taylor series expansion is the same as that discussed in the linear oblique interface case, but the local coordinate transformation and the formulas for interface conditions need to be modified. The coordinate transformation is no longer simply the rotation transformation, and we set up a local cylindrical coordinate system. The position of the origin O' of the local cylindrical coordinate system is determined by the point where we match the interface conditions, the normal and tangential unit vectors $\hat{\rho}$ and $\hat{\phi}$, and the effective radius R, as shown in Fig. 3. The transformation is more complicated than those in

the linear oblique interface case, and the field components and their derivatives with respect to ρ and ϕ are given as follows:

$$\begin{aligned}
\psi_x &= \cos\phi\cdot\psi_\rho - \sin\phi\cdot\psi_\phi \\
\psi_y &= \sin\phi\cdot\psi_\rho + \cos\phi\cdot\psi_\phi \\
\frac{\partial\psi_x}{\partial x} &= \frac{\sin^2\phi}{R}\psi_\rho + \cos^2\phi\frac{\partial\psi_\rho}{\partial\rho} - \frac{\sin\phi\cos\phi}{R}\frac{\partial\psi_\rho}{\partial\phi} \\
&\quad + \frac{\sin\phi\cos\phi}{R}\psi_\phi - \sin\phi\cos\phi\frac{\partial\psi_\phi}{\partial\rho} + \frac{\sin^2\phi}{R}\frac{\partial\psi_\phi}{\partial\phi} \\
\frac{\partial\psi_x}{\partial y} &= -\frac{\sin\phi\cos\phi}{R}\psi_\rho + \sin\phi\cos\phi\frac{\partial\psi_\rho}{\partial\rho} + \frac{\cos^2\phi}{R}\frac{\partial\psi_\rho}{\partial\phi} \\
&\quad - \frac{\cos^2\phi}{R}\psi_\phi - \sin^2\phi\frac{\partial\psi_\phi}{\partial\rho} - \frac{\sin\phi\cos\phi}{R}\frac{\partial\psi_\phi}{\partial\phi} \\
\frac{\partial\psi_y}{\partial x} &= -\frac{\sin\phi\cos\phi}{R}\psi_\rho + \sin\phi\cos\phi\frac{\partial\psi_\rho}{\partial\rho} - \frac{\sin^2\phi}{R}\frac{\partial\psi_\rho}{\partial\phi} \\
&\quad + \frac{\sin^2\phi}{R}\psi_\phi + \cos^2\phi\frac{\partial\psi_\phi}{\partial\rho} - \frac{\sin\phi\cos\phi}{R}\frac{\partial\psi_\phi}{\partial\phi} \\
\frac{\partial\psi_y}{\partial y} &= \frac{\cos^2\phi}{R}\psi_\rho + \sin^2\phi\frac{\partial\psi_\rho}{\partial\rho} + \frac{\sin\phi\cos\phi}{R}\frac{\partial\psi_\rho}{\partial\phi} \\
&\quad - \frac{\sin\phi\cos\phi}{R}\psi_\phi + \sin\phi\cos\phi\frac{\partial\psi_\phi}{\partial\rho} + \frac{\cos^2\phi}{R}\frac{\partial\psi_\phi}{\partial\phi} \\
&\vdots
\end{aligned}$$

Compared with those for the linear oblique interface case, the complexity of the above equations results from the partial differential operation with respect to ϕ and ρ in the local cylindrical coordinate. The above transformation can also be expressed in a linear equation form as in (12). We can also transform the quantities from the ρ–ϕ local coordinate system back to the x–y global coordinate system in a similar manner as

$$\begin{aligned}
\psi_\rho &= \cos\phi\cdot\psi_x + \sin\phi\cdot\psi_y \\
\psi_\phi &= -\sin\phi\cdot\psi_x + \cos\phi\cdot\psi_y \\
\frac{\partial\psi_\rho}{\partial\rho} &= \cos^2\phi\frac{\partial\psi_x}{\partial x} + \sin\phi\cos\phi\frac{\partial\psi_x}{\partial y} + \sin\phi\cos\phi\frac{\partial\psi_y}{\partial x} \\
&\quad + \sin^2\phi\frac{\partial\psi_y}{\partial y} \\
\frac{\partial\psi_\rho}{\partial\phi} &= -\sin\phi\psi_x - R\sin\phi\cos\phi\frac{\partial\psi_x}{\partial x} + R\cos^2\phi\frac{\partial\psi_x}{\partial y} \\
&\quad + \cos\phi\psi_y - R\sin^2\phi\frac{\partial\psi_y}{\partial x} + R\sin\phi\cos\phi\frac{\partial\psi_y}{\partial y} \\
\frac{\partial\psi_\phi}{\partial\rho} &= -\sin\phi\cos\phi\frac{\partial\psi_x}{\partial x} - \sin^2\phi\frac{\partial\psi_x}{\partial y} + \cos^2\phi\frac{\partial\psi_y}{\partial x} \\
&\quad + \sin\phi\cos\phi\frac{\partial\psi_y}{\partial y} \\
\frac{\partial\psi_\phi}{\partial\phi} &= -\cos\phi\psi_x + R\sin^2\phi\frac{\partial\psi_x}{\partial x} - R\sin\phi\cos\phi\frac{\partial\psi_x}{\partial y} \\
&\quad - \sin\phi\psi_y - R\sin\phi\cos\phi\frac{\partial\psi_y}{\partial x} + R\cos^2\phi\frac{\partial\psi_y}{\partial y} \\
&\vdots
\end{aligned}$$

or expressed in a matrix form similar to (13). The interface conditions in the local cylindrical coordinate system are different from those in the linear oblique interface case. Their expressions are given as follows:

$$\begin{aligned}
H_\rho|_R &= H_\rho|_L \\
H_\phi|_R &= H_\phi|_L \\
\left.\frac{\partial H_\rho}{\partial\rho}\right|_R &= \left.\frac{\partial H_\rho}{\partial\rho}\right|_L \\
\left.\frac{\partial H_\rho}{\partial\phi}\right|_R &= \left.\frac{\partial H_\rho}{\partial\phi}\right|_L \\
\left.\frac{\partial H_\phi}{\partial\rho}\right|_R &= \frac{\epsilon_R}{\epsilon_L}\left.\frac{\partial H_\phi}{\partial\rho}\right|_L + \frac{1-\frac{\epsilon_R}{\epsilon_L}}{R}\left.\frac{\partial H_\rho}{\partial\phi}\right|_L \\
&\quad - \frac{1-\frac{\epsilon_R}{\epsilon_L}}{R}H_\phi|_L \\
\left.\frac{\partial H_\phi}{\partial\phi}\right|_R &= \left.\frac{\partial H_\phi}{\partial\phi}\right|_L \\
\left.\frac{\partial^2 H_\rho}{\partial\rho^2}\right|_R &= \left.\frac{\partial^2 H_\rho}{\partial\rho^2}\right|_L + k_0^2(\epsilon_L-\epsilon_R)H_\rho|_L \\
\left.\frac{\partial^2 H_\phi}{\partial\rho^2}\right|_R &= \left.\frac{\partial^2 H_\phi}{\partial\rho^2}\right|_L + \left[k_0^2(\epsilon_L-\epsilon_R) + \frac{1-\frac{\epsilon_R}{\epsilon_L}}{R^2}\right]H_\phi|_L \\
&\quad + \frac{1-\frac{\epsilon_R}{\epsilon_L}}{R}\left.\frac{\partial H_\phi}{\partial\rho}\right|_L - \frac{1-\frac{\epsilon_R}{\epsilon_L}}{R^2}\left.\frac{\partial H_\rho}{\partial\phi}\right|_L \\
&\vdots \\
E_\rho|_R &= \frac{\epsilon_L}{\epsilon_R}E_\rho|_L \\
E_\phi|_R &= E_\phi|_L \\
\left.\frac{\partial E_\rho}{\partial\rho}\right|_R &= \left.\frac{\partial E_\rho}{\partial\rho}\right|_L + \frac{1-\frac{\epsilon_R}{\epsilon_L}}{R}E_\rho|_L \\
\left.\frac{\partial E_\rho}{\partial\phi}\right|_R &= \frac{\epsilon_L}{\epsilon_R}\left.\frac{\partial E_\rho}{\partial\phi}\right|_L \\
\left.\frac{\partial E_\phi}{\partial\rho}\right|_R &= \left.\frac{\partial E_\phi}{\partial\rho}\right|_L + \frac{\frac{\epsilon_L}{\epsilon_R}-1}{R}\left.\frac{\partial E_\rho}{\partial\phi}\right|_L \\
\left.\frac{\partial E_\phi}{\partial\phi}\right|_R &= \left.\frac{\partial E_\phi}{\partial\phi}\right|_L \\
\left.\frac{\partial^2 E_\rho}{\partial\rho^2}\right|_R &= \frac{\epsilon_L}{\epsilon_R}\left.\frac{\partial^2 E_\rho}{\partial\rho^2}\right|_L + \frac{\frac{\epsilon_L}{\epsilon_R}-1}{R}\left.\frac{\partial E_\rho}{\partial\rho}\right|_L \\
&\quad + \left[\frac{k_0^2\epsilon_L(\epsilon_L-\epsilon_R)}{\epsilon_R} + \frac{\frac{\epsilon_L}{\epsilon_R}-1}{R^2}\right]E_\rho|_L \\
\left.\frac{\partial^2 E_\phi}{\partial\rho^2}\right|_R &= \left.\frac{\partial^2 E_\phi}{\partial\rho^2}\right|_L + k_0^2(\epsilon_L-\epsilon_R)E_\phi|_L \\
&\quad + \frac{1-\frac{\epsilon_L}{\epsilon_R}}{R^2}\left.\frac{\partial E_\rho}{\partial\phi}\right|_L \\
&\vdots
\end{aligned}$$

for the magnetic fields and the electric fields, respectively. The interface conditions can be rewritten in a matrix form as in (14). It is worth noticing that the curved interface will introduce different amounts of coupling between the two polarizations of the field compared with that in the case of linear oblique interface case. The other procedure of derivation is the same as that in the linear oblique interface case, leading to expressions similar to (15)–(17).

III. Implementation

Substituting the resultant FD formulas derived in Section II into the Helmholtz equation

$$\psi'' + k_0^2 \epsilon \psi = \beta^2 \psi \tag{18}$$

for x and y polarizations of the field, respectively, at the sampled point (m, n) leads to

$$\mathbf{M} \cdot \begin{bmatrix} \psi_x|_{(m-1,n+1)} \\ \vdots \\ \psi_x|_{(m+1,n-1)} \\ \psi_y|_{(m-1,n+1)} \\ \vdots \\ \psi_y|_{(m+1,n-1)} \end{bmatrix} + k_0^2 \epsilon_{(m,n)} \begin{bmatrix} \psi_x|_{(m,n)} \\ \psi_y|_{(m,n)} \end{bmatrix} = \beta^2 \begin{bmatrix} \psi_x|_{(m,n)} \\ \psi_y|_{(m,n)} \end{bmatrix} \tag{19}$$

where $\mathbf{M}$ is a 2×18 matrix containing entries obtained from the derived new FD formulas, and $\epsilon_{(m,n)}$ denotes the relative permittivity at the point (m, n). By assembling the fields at all sampled points in the computation domain as $\mathbf{\Psi} = [\psi_x|_{(0,0)}, \psi_x|_{(1,0)}, \ldots \psi_x|_{(M,N)}, \psi_y|_{(0,0)}, \ldots \psi_y|_{(M,N)}]^t$ and applying (19) together with suitable boundary conditions, we obtain an algebraic eigenvalue equation

$$\left[\mathbf{A} + k_0^2 \mathbf{E}\right] \mathbf{\Psi} = \beta^2 \mathbf{\Psi} \tag{20}$$

or denoted as

$$\widetilde{\mathbf{A}} \mathbf{\Psi} = \beta^2 \mathbf{\Psi} \tag{21}$$

where $\widetilde{\mathbf{A}} = \mathbf{A} + k_0^2 \mathbf{E}$, $\mathbf{E} = \mathrm{diag}(\epsilon_{(0,0)}, \epsilon_{(1,0)}, \ldots \epsilon_{(m,n)}, \ldots)$, and $\mathbf{A}$ results from the operator $\partial^2/\partial x^2 + \partial^2/\partial y^2$ on ψ and its elements can be obtained from the elements of the matrix $\mathbf{M}$. The eigenvalue probelm of (21) can be solved with the shifted-inverse power method (SIPM) [10]. Because the resultant matrix $\widetilde{\mathbf{A}}$ will be nonsymmetric in the vectorial case, we adopt BiCGSTAB [11] to solve the matrix inverse operation. To evaluate the eigenvalue, we apply the Rayleigh quotient formula

$$\beta^2 = \frac{\mathbf{\Psi^t} \widetilde{\mathbf{A}} \mathbf{\Psi}}{\mathbf{\Psi^t} \mathbf{\Psi}}. \tag{22}$$

Because the resultant fields are confined fields in our calculation, we choose the transparent boundary condition (TBC) [12], [13] at the boundary of our computational window.

For a 2-D problem with N total mesh points in the computational domain, the resultant matrix of the corresponding eigenvalue problem will be a $2N \times 2N$ one. If we adopt the conventional five-point FD scheme, the storage memory required will be $10 \times (2N)$ only. In our method, we still employ the five-point formulas in the homogeneous region, but we need to use at least nine points to obtain correct formulas at the interface. Thus, the memory requirement of our method for a general case will be $18 \times (2N)$. However, since most of the mesh points are located in the homogeneous regions, the memory requirement can be practically reduced to $10 \times (2N) + 4K$ with an appropriate programming technique, where K is the number of mesh points at the interface. We have computed the same problem using both the conventional formulation and our new formulation with the same programming algorithm on the same computer and have found that the run time of our method is only 10%–20% longer than that of the conventional method. Again, the reason is that most of the mesh points belong to the homogeneous regions where our formulation reduces to the conventional one, and the only extra effort in our method is that we need to solve an 18×18 matrix inversion at every interface mesh point.

IV. Numerical Results

A. Assessment of the Formulation

To validate the method presented above, we choose a step-index fiber as an example since the exact analytical solutions are known. The parameters we choose for a multimode fiber are as follows: the core diameter $d = 15$ μm, the refractive index of the core $n_{\mathrm{co}} = 1.47$, the refractive index of the cladding $n_{\mathrm{clad}} = 1.46$, and the operating wavelength $\lambda = 1.55$ μm. These parameters are the same as those used by Xu *et al.* [5]. Xu *et al.* calculated the same problem using the conventional full-vectorial FD method with the graded-index approximation expressed in (2)–(5).

We calculate the fundamental HE_{11} mode and the higher order TE_{01} mode and compare them with the analytical solutions. The convergence of the numerical solutions is evaluated by reducing the mesh size. Fig. 4(a) shows the percentage error in the normalized propagation constant versus the mesh size ($\Delta x = \Delta y$) for the different modes. The exact propagation constants of this waveguide are 5.952 859 930 9 $\mu\mathrm{m}^{-1}$ and 5.943 809 559 9 $\mu\mathrm{m}^{-1}$ for the HE_{11} and TE_{01} modes, respectively. The percentage error in the normalized propagation constant is calculated as

$$\text{error, } \% = \left| \frac{\tilde{\beta}_{\mathrm{calculated}} - \tilde{\beta}_{\mathrm{exact}}}{\tilde{\beta}_{\mathrm{exact}}} \right| \times 100 \tag{23}$$

with the normalized propagation constant defined by $\tilde{\beta} = (n_{\mathrm{co}}\beta - n_{\mathrm{clad}}k_0)/(n_{\mathrm{co}}k_0 - n_{\mathrm{clad}}k_0)$. We perform the calculation using the following four formulations: H-fields with a curved interface, E-fields with a curved interface, H-fields with a linear oblique interface, and E-fields with a linear oblique interface. We also show the results reported by Xu *et al.* [5] in Fig. 4(a) for comparison. It is seen that, for both the fundamental and the higher order modes, numerical results converge to the exact solutions as the mesh size decreases, and in both cases our results converge more rapidly compared to those of [5]. In most of the cases, the accuracy of these four kinds of formulations are of the same order except that the accuracy of the E-formulation with the linear oblique interface appears to be worse than its corresponding H-formulation. This can be explained by the discontinouity of the E-field which introduces extra errors in the process of matching interface conditions with a linear oblique interface approximation. On the other hand, we also find that the error is particularly small in the HE_{11} mode case obtained by the H-formulation with a curved interface. In the HE_{11} mode case, it is found that the ratio between the two orthogonal transverse field components (e.g., E_x and E_y) is over one thousand. Therefore, the HE_{11}

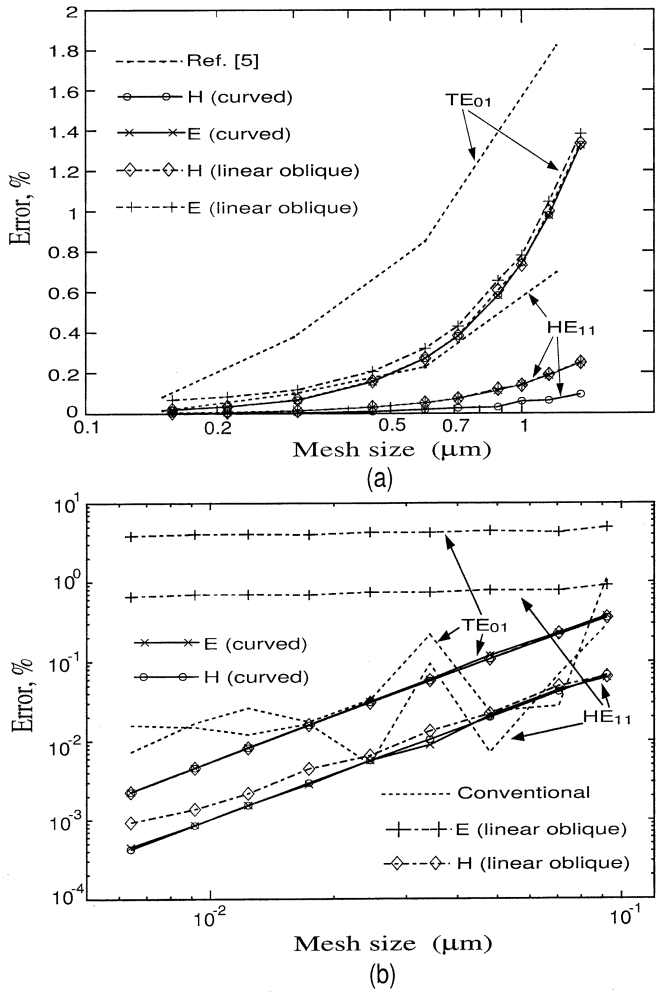

Fig. 4. Percentage error in the normalized propagation constant for the HE_{11} and TE_{01} modes of the step-index optical fiber as a function of the mesh size $\Delta x = \Delta y$. (a) $d = 15\ \mu$m, $n_{\mathrm{co}} = 1.47$, $n_{\mathrm{clad}} = 1.46$, and $\lambda = 1.55\ \mu$m. (b) $d = 0.6\ \mu$m, $n_{\mathrm{co}} = \sqrt{8}$, $n_{\mathrm{clad}} = 1$, and $\lambda = 1.5\ \mu$m.

mode is very close to the scalar LP_{01} mode and can be calculated accurately by either scalar or semivectorial formulation. However, as mentioned in [5], in the TE_{01} mode case the two transverse field components have amplitudes of the same order, and it cannot be accurately analyzed by the scalar or semivectorial method since neither of the two components is negligible.

In our formulations, it can be found that the differences in the refractive index and in the curvature of the interface significantly influence the accuracy of the calculated results. The difference in the refractive index in the case of Fig. 4(a) is only 0.01, and, with the core diameter of 15 μm, the graded-index approximation could be still valid. We consider a strongly guiding case for comparison. The parameters chosen are d (the core diameter) $= 1.2\ \mu$m, $n_{\mathrm{co}} = \sqrt{8}$, $n_{\mathrm{clad}} = 1.0$, and $\lambda = 1.5\ \mu$m. The exact propagation constants of this waveguide are 11.242 793 843 78 and 10.483 439 431 95 $\mu\mathrm{m}^{-1}$ for the HE_{11} and TE_{01} modes, respectively. Fig. 4(b) shows the percentage error in the normalized propagation constant versus the mesh size, again for the HE_{11} and TE_{01} modes. The results are now presented in log scale along both axes. It is seen that the E-formulation with the linear oblique interface assumption does not give convergent results because the discontinuity of the field in the interface conditions is treated across the approximate linear interface rather than across the real curved boundary. However, the results obtained by the H-field formulation with linear oblique interface assumptions still converge to the analytical results due to the continuity of the fields, and its order of truncation error is also close to two. The error of results calculated by (1)–(5) based on the conventional graded-index approximation is on the order of 10^{-2} and does not converge to the analytical results. Both E- and H-formulations with curved interface uniformly converge to the analytical solutions for both the HE_{11} and TE_{01} modes with an order-of-two truncation error.

Figs. 5 and 6 plot patterns of the two transverse electric field components of the HE_{11} mode and the TE_{01} mode, respectively, for the case of Fig. 4(b). We find that the ratio between the maximum amplitudes of the two transverse field components of the HE_{11} mode $(E_y{:}E_x)$ is about 1:0.0593 in Fig. 5, and an analysis using scalar or semivectorial formulations would cause significant error. As can be seen in Fig. 5, the amplitude maximum of E_y is at the center of the fiber, while those of E_x are located at the internal edge of the fiber where the normalized amplitude of the dominant field E_y are about 0.0938. As for the TE_{01} mode shown in Fig. 6, the ratio between the maximum amplitudes of E_x and E_y is almost 1:1 with an accuracy to the seventh digit. The fields at the interface for the TE_{01} mode are continuous since the only component of the transverse field is E_ϕ which is continuous at the interface. The contour profiles of the fields obtained by our curved interface formulation appear to be smoothly continuous at the interface, as shown in Fig. 6. The contour behaviors of the fields at the interface are still accurate even for the case with large refractive index difference.

B. Application to Fused Fiber-Optic Couplers

The fused fiber-optic coupler is an important device in optical communication systems [14]. It can be designed as a power splitter, a polarization beamsplitter, and other devices [15]. The characteristics of the fused fiber-optic coupler have been carefully studied by employing SIEM [16], [17]. Here we calculate the modal quantities, including the propagation constants, the coupling coefficients, and the form birefringence of the fused fiber-optic coupler using our proposed formulation and compare the results with those given in [17]. The cross-sectional view of the structure is shown in Fig. 7(a) and the parameters considered are as follows: the core index $n_{\mathrm{co}} = 1.45$, the cladding index $n_{\mathrm{clad}} = 1$, the operating wavelength $\lambda = 1.523\ \mu$m, the aspect ratio $2d/2r = 1.8$, where r is the radius of the individual core, and the normalized frequency $V \equiv (2\pi/\lambda)\cdot r\cdot\sqrt{n_{\mathrm{co}}^2 - n_{\mathrm{clad}}^2} = 50$. These parameters are the same as those used in [17]. We calculate the propagation constants of the lowest order even and odd modes of x and y polarizations, β_{even}^x, β_{even}^y, β_{odd}^x, and β_{odd}^y, where the even or odd mode is defined according to whether its main component of the magnetic field is symmetrical or antisymmetrical about the y axis, and the polarization direction is defined as the main direction of the electric field. The coupling coefficient of the i polarization state, C_i ($i = x$ or

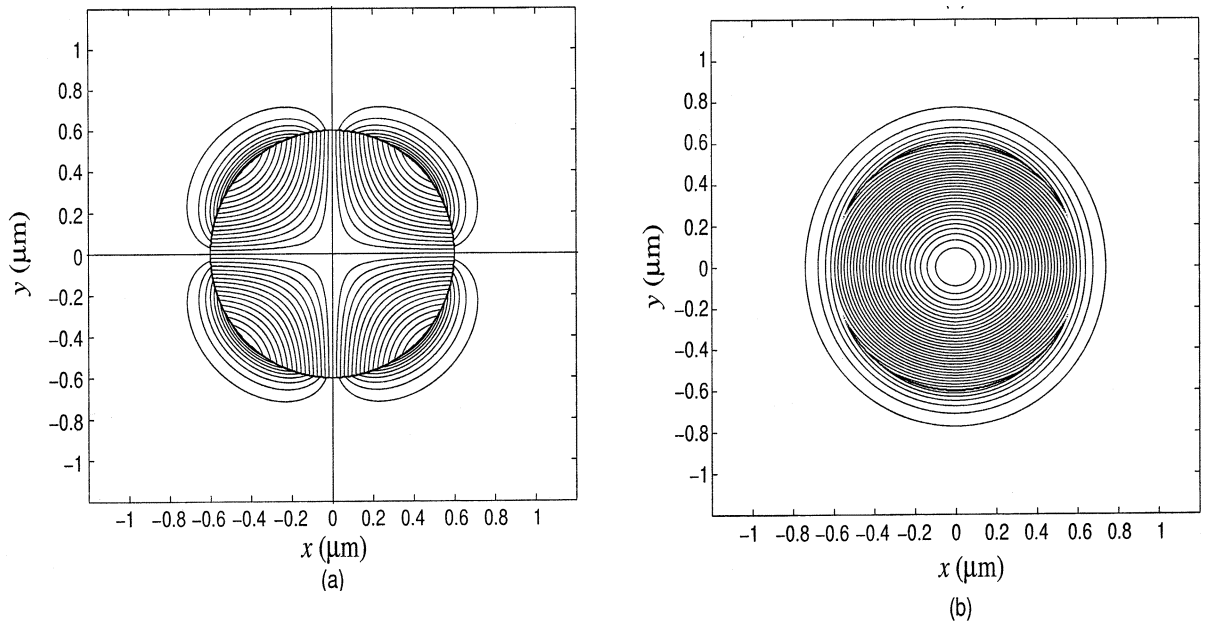

Fig. 5. Electric filed patterns of the HE_{11} mode. (a) E_x component. (b) E_y component.

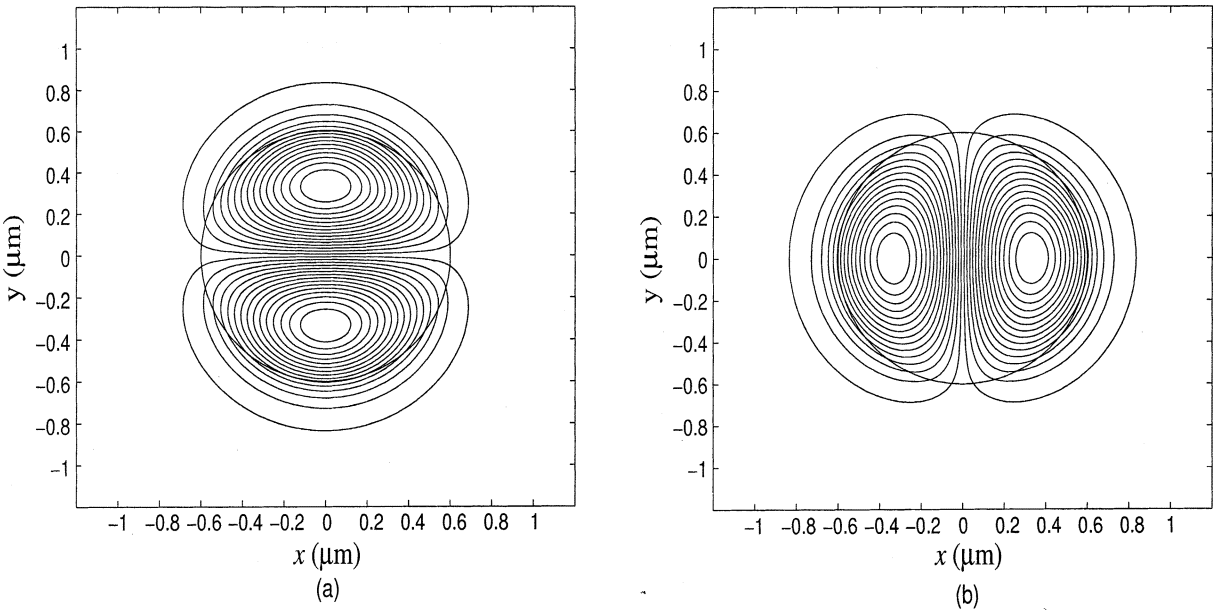

Fig. 6. Electric filed patterns of the TE_{01} mode. (a) E_x component. (b) E_y component.

y), is defined as $C_i \equiv (\beta^i_{\mathrm{even}} - \beta^i_{\mathrm{odd}})/2$ and the form birefringence is defined as $B \equiv (rV^2/\Delta^{3/2})(C_x - C_y)$ where $\Delta = (n^2_{\mathrm{co}} - n^2_{\mathrm{clad}})/2n^2_{\mathrm{co}}$. The coupling coefficient decides the coupling strength of the coupler and the form birefringence causes the polarization splitting behavior. As mentioned in [17], the form birefringence is very small, and achieving an accurate caculation of such a small quantity is quite difficult.

The converged normalized propagation constants of the first four modes caculated by the SIEM [17] are $\beta^x_{\mathrm{even}} = 0.998\,298\,295\ \mu\mathrm{m}^{-1}$, $\beta^y_{\mathrm{even}} = 0.998\,287\,649\ \mu\mathrm{m}^{-1}$, $\beta^x_{\mathrm{odd}} = 0.997\,581\,191\ \mu\mathrm{m}^{-1}$, and $\beta^y_{\mathrm{odd}} = 0.997\,574\,799\ \mu\mathrm{m}^{-1}$. Also, the corresponding normalized coupling coefficients and the form birefringence are $rC_x = 0.006\,494\,5$, $rC_y = 0.006\,455\,5$, and $B = 0.727\,627$. These results were calculated by using very fine boundary meshes. Since the field patterns of the lowest four modes in each individual fiber of the fused coupler are similar to that of the HE_{11} mode in a single optical fiber and the H-formulation with curved interface is particularly accurate in this case, we choose this formulation for making the comparison. The numerical results obtained using our improved formulations are shown in Tables I and II and the field patterns of these four modes are shown in Fig. 7(b)–(e). As indicated in [17], detailed calculation of the fields at the sharp corner of the dumbbell-shaped cross section significantly affects the accuracy of the computed propagation constants and related coupling quantities, and using nonuniform division near the corner can improve the efficiency of computation. We also use the nonuniform division scheme in the improved FD calculation, and $\Delta x_{\min}$ and $\Delta x_{\max}$ in Table II represent the minmum and maxmum division grids, respectively, in the calculation. The computational domain in our calculation includes only one quarter of the dumbell-shaped cross section

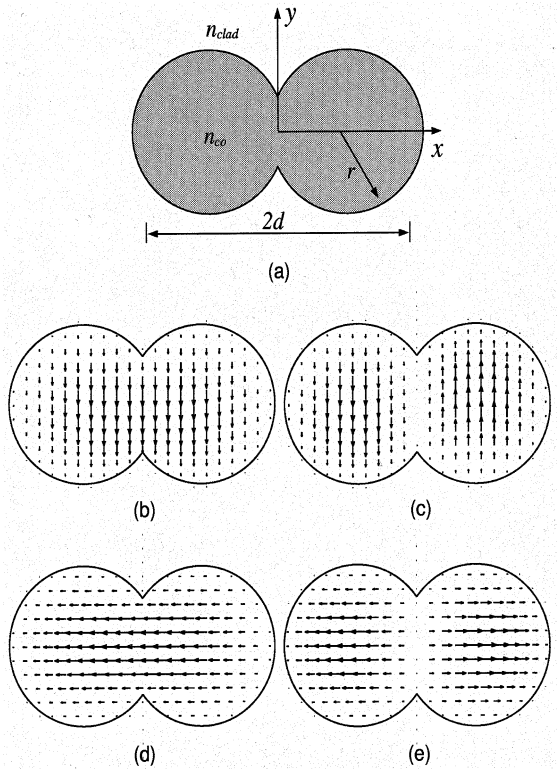

Fig. 7. (a) Cross-sectional view of the fused fiber-optic coupler. (b)–(e) Magnetic field patterns of the lowest four mode of the fused optic-fiber coupler: (b) x-polarized even mode, (c) x-polarized odd mode, (d) y-polarized even mode, and (e) y-polarized odd mode.

TABLE I
CONVERGENCE CHARACTERISTICS OF PROPAGATION CONSTANTS OF THE FIRST FOUR MODES BY THE PROPOSED FORMULATION WITH NONUNIFORM DIVISION

Δx_{min} (μm)	$N_x \times N_y$	β^x_{even} (μm^{-1})	β^y_{even} (μm^{-1})	β^y_{even} (μm^{-1})	β^y_{odd} (μm^{-1})
0.04	69× 65	0.998302537	0.998290552	0.997585419	0.997580656
0.04	125× 90	0.998300907	0.998289193	0.997582567	0.997576332
0.04	188×122	0.998300646	0.998289049	0.997582116	0.997575827
0.02	98× 88	0.998301021	0.998288732	0.997584475	0.997577563
0.02	196×137	0.998299801	0.998288286	0.997582252	0.997575811
0.02	292×187	0.998299405	0.998288236	0.997581985	0.997575585
0.01	143×125	0.998299697	0.998288173	0.997582974	0.997576355
0.01	207×157	0.998299217	0.998288078	0.997582242	0.997575763
0.01	303×207	0.998299026	0.998288044	0.997581967	0.997575566
0.005	253×188	0.998298995	0.998287902	0.997582016	0.997575548
0.005	307×216	0.998298924	0.998287924	0.997581929	0.997575552
0.005	370×251	0.998298858	0.998287980	0.997581893	0.997575498
0.003	437×297	0.998298803	0.998287976	0.997581862	0.997575478

using the symmetry conditions of the fields. The symbols N_x and N_y in Tables I and II denote the numbers of divisions in x and y directions, respectively, in our calculation. We model the sharp corner as a small section of arc with a very small effective radius. The curvature would influence the calculated field behavior, as indicated in the discussion of the curved interface formulations. We find that, as $\Delta x_{\min}$ near the corner decreases, the result converges to that given in [17]. We also observe that the form birefringence still does not reach a stable value as the number of divisons increase, although the propagation constants converge. To obtain a convergent value of the form birefringence, the propagation constants of the lowest four modes have to converge to the sixth significant digit and the coupling coefficients of both polarization states to at least the third significant digit. Our results generally compare with those of [17] to within 0.0001%, 0.04%, and 3% for the normalized propagation constants, the coupling coefficients, and the form birefringence, respectively. The consistency of our results with those calculated by the SIEM further supports the accuracy of the proposed improved FD method.

TABLE II
CONVERGENCE CHARACTERISTICS OF COUPLING COEFFICENTS AND FORM BIREFRINGENCE BY THE PROPOSED FORMULATION WITH NONUNIFORM DVISION

Δx_{min} (μm)	Δx_{max} (μm)	$N_x \times N_y$	rC_x	rC_y	B
0.04	0.45	69× 65	0.0064824	0.0064171	1.2224
0.04	0.2	125× 90	0.0064935	0.0064439	0.9272
0.04	0.125	188×122	0.0064952	0.0064472	0.8982
0.02	0.3	98× 88	0.0064895	0.0064408	0.9065
0.02	0.125	196×137	0.0064967	0.0064526	0.8199
0.02	0.08	292×187	0.0064974	0.0064542	0.8039
0.01	0.2	143×125	0.0064911	0.0064467	0.8269
0.01	0.125	207×157	0.0064934	0.0064512	0.7856
0.01	0.08	303×207	0.0064941	0.0064527	0.7721
0.005	0.1	253×188	0.0064934	0.0064515	0.7797
0.005	0.08	307×216	0.0064936	0.0064525	0.7641
0.005	0.065	370×251	0.0064933	0.0064527	0.7559
0.003	0.055	437×297	0.0064930	0.0064528	0.7491

V. SUMMARY AND CONCLUDING REMARKS

We have derived improved FD formulas for solving full-vectorial modes of step-index optical waveguides. A general relation is derived from the Taylor series expansion, the local coordinate transformation, and matching the interface conditions. The formulation is a full-vectorial one and the only truncation error is not from matching the interface conditions but from the truncation of the higher order terms in the Taylor series expansion. The interface in the structure is allowed to be oblique to the coordinate axes and even to be curved, thus our formulation is flexible for dealing with step-index boundaries of arbitrary shape.

The improved formulation has been applied to calculate the fundamental HE_{11} mode and the higher order TE_{01} mode of a step-index fiber, and the results have been compared with exact analytical solutions and those of [5] which involve the graded-index approximation. It is found that our results converge to the exact analytical solutions and are better than those of [5]. We have also applied our new formulation to the analysis of the fused fiber-optic coupler. By comparing our results with those calculated using the SIEM [17], it is found that our new formulation can be used to compute such quantities as the form birefringence which must be determined from calculated propagation characteristics of very high accuracy.

The example of the fused fiber-optic coupler contains a sharp corner in its cross section, although it is located at the boundary of the computaional domain after using the mode field symmetry. We have modeled the corner as a small section of arc with a very small effective radius. For optical waveguides in integrated optical devices, e.g., rib waveguides, the waveguide cross section often contains (90°) corners. Field singularities would appear at such corners and cause difficulty in full-vectorial mode solutions [18], [19]. We can again model the corner as

a tiny section of arc, use the curved interface formulations proposed in this paper, and adopt nonuniform division in the FD mode solution. We have studied such problems and found that the calculated field behaves like a singular one as the effective radius of the arc is made to be much smaller. The results will be reported in a separate publication.

REFERENCES

[1] M. S. Stern, "Semivectorial polarized finite difference method for optical waveguides with arbitrary index profiles," *Proc. Inst. Elect. Eng.*, pt. J, vol. 135, pp. 56–63, 1988.

[2] C. Vassallo, "Improvement of finite difference methods for step-index optical waveguides," *Proc. Inst. Elect. Eng.*, pt. J, vol. 139, pp. 137–142, 1992.

[3] J. Yamauchi, M. Sekiguchi, O. Uchiyama, J. Shibayama, and H. Nakano, "Modified finite-difference formula for the analysis of semivectorial modes in step-index optical waveguides," *IEEE Photon. Technol. Lett.*, vol. 9, pp. 961–963, July, 1997.

[4] A. P. Ansbro and I. Montrosset, "Vectorial finite difference scheme for isotropic dielectric waveguides: Transverse electric field representation," *Proc. Inst. Elect. Eng.*, pt. J, vol. 140, pp. 253–259, 1993.

[5] C. L. Xu, W. P. Huang, M. S. Stern, and S. K. Chaudhuri, "Full-vectorial mode calculations by finite difference method," *Proc. Inst. Elect. Eng.*, pt. J, vol. 141, pp. 281–286, 1994.

[6] G. R. Hadley and R. E. Smith, "Full-vector waveguide modeling using an iterative finite-difference method with transparent boundary conditions," *J. Lightwave Technol.*, vol. 13, pp. 465–469, Mar. 1995.

[7] S. Sujecki, T. M. Benson, P. Sewell, and P. C. Kendall, "Novel vectorial analysis of optical waveguides," *J. Lightwave Technol.*, vol. 16, pp. 1329–1335, July 1998.

[8] J. Yamauchi, G. Takahashi, and H. Nakano, "Full-vectorial beam-propagation method based on the McKee-Mitchell scheme with improved finite-difference formulas," *J. Lightwave Technol.*, vol. 16, pp. 2458–2464, Dec. 1998.

[9] Y.-P. Chiou, Y.-C. Chiang, and H.-C. Chang, "Improved three-point formulas considering the interface conditions in the finite-difference analysis of step-index optical devices," *J. Lightwave Technol.*, vol. 18, pp. 243–251, Feb., 2000.

[10] A. Jennings, *Matrix Computation for Engineers and Scientists*. New York: Wiley, 1977.

[11] H. A. van der Vorst, "Bi-CGSTAB: A fast and smoothly converging variant of Bi-CG for the solution of nonsymmetric linear system," *SIAM J. Sci. Statist. Comput.*, vol. 13, pp. 631–644, 1992.

[12] G. R. Hadley, "Transparent boundary condition for the beam propagation method," *IEEE J. Quantum Electron.*, vol. 28, pp. 363–370, Jan., 1992.

[13] C. Vassallo and J. M. van der Keur, "Comparison of a few transparent boundary conditions for finite-difference optical mode-solvers," *J. Lightwave Technol.*, vol. 15, pp. 397–402, Feb. 1997.

[14] B. S. Kawasaki, K. O. Hill, and R. G. Lamont, "Biconical-taper single-mode fiber coupler," *Opt. Lett.*, vol. 6, pp. 327–328, 1981.

[15] M. Eisenmann and E. Weidel, "Single-mode fused biconical coupler optimized for polarization beamsplitting," *J. Lightwave Technol.*, vol. 9, pp. 853–858, July 1991.

[16] T.-L. Wu and H.-C. Chang, "Vectorial analysis of form birefringence of weakly fused fiber-optic couplers," *J. Lightwave Technol.*, vol. 13, pp. 687–691, Apr. 1995.

[17] S.-W. Yang and H.-C. Chang, "Numerical modeling of weakly fused fiber-optic polarization beamsplitters—Part I: Accurate calculation of coupling coefficients and form birefringence," *J. Lightwave Technol.*, vol. 16, pp. 685–690, Apr. 1998.

[18] W. W. Lui, C.-L. Xu, W.-P. Huang, K. Yokoyama, and S. Seki, "Full-vectorial mode analysis with considerations of field singularities at corners of optical waveguides," *J. Lightwave Technol.*, vol. 17, pp. 1509–1513, Aug. 1999.

[19] D.-U. Li and H.-C. Chang, "An efficient full-vectorial finite element modal analysis of dielectric waveguides incorporating inhomogeneous elements across dielectric discontinuities," *IEEE J. Quantum Electron.*, vol. 36, pp. 1251–1261, Nov. 2000.

Yen-Chung Chiang was born in Hualien, Taiwan, on March 10, 1970. He received the B.S. and M.S. degrees in electrical engineering from National Taiwan University, Taipei, in 1992 and 1994, respectively. He is currently working toward the Ph.D. degree at the same university.

His research interests include numerical methods for solving optical waveguide problems.

Yih-Peng Chiou was born in Taoyuan, Taiwan, in 1969. He received the B.S. and Ph.D. degrees from National Taiwan University, Taipei, in 1992 and 1998, respectively, both in electrical engineering. His Ph.D. dissertation was on the numerical techniques of guided wave structures.

From 1999 to 2000, he was with the Taiwan Semiconductor Manufacturing Company, where his interest was the plasma enhanced chemical vapor deposition of dielectric films. In 2001, he joined Rsoft Inc., Ossining, NY, where he currently acts as a Staff Scientist, developing the design tools and supporting the customers in designing. His research interests include the numerical techniques of guided wave structures and the theory, design, and application of communication devices and photonic crystal structures.

Hung-Chun Chang (S'78–M'83–SM'00) was born in Taipei, Taiwan, on February 8, 1954. He received the B.S. degree from National Taiwan University, Taipei, in 1976 and the M.S. and Ph.D. degrees from Stanford University, Stanford, CA, in 1980 and 1983, respectively, all in electrical engineering.

From 1978 to 1984, he was with the Space, Telecommunications, and Radioscience Laboratory of Stanford University. In August 1984, he joined the faculty of the Electrical Engineering Department, National Taiwan University, where he is currently a Professor. He served as Vice-Chairman of the Electrical Engineering Department from 1989 to 1991, and Chairman of the newly-established Graduate Institute of Electro-Optical Engineering at the same university from 1992 to 1998. His current research interests include the theory, design, and application of guided-wave structures and devices for fiber optics, integrated optics, optoelectronics, and microwave and millimeter-wave circuits.

Dr. Chang is a Member of Sigma Xi, the Phi Tan Phi Scholastic Honor Society, the Chinese Institute of Engineers, the Photonics Society of Chinese-Americans, the Optical Society of America, the Electromagnetics Academy, and China/SRS (Taipei) National Committee (a Standing Committee member during 1988–1993) and Commission H of the U.S. National Committee of the International Union of Radio Science (URSI). In 1987, he was among the recipients of the Young Scientists Award at the URSI XXIInd General Assembly. In 1993, he was one of the recipients of the Distinguished Teaching Award sponsored by the Ministry of Education of the Republic of China.